

Spectroscopic Evidence of the Aharonov-Casher effect in a Cooper Pair Box

M.T. Bell^{1,2}, W. Zhang¹, L.B. Ioffe^{1,3}, and M.E. Gershenson¹

¹*Department of Physics and Astronomy, Rutgers University,
136 Frelinghuysen Rd., Piscataway, NJ 08854, USA*

²*Department of Electrical Engineering, University of Massachusetts, Boston, Massachusetts 02125 and*

³*LPTHE, CNRS UMR 7589, 4 place Jussieu, 75252 Paris, France*

We have observed the effect of the Aharonov-Casher (AC) interference on the spectrum of a superconducting system containing a symmetric Cooper pair box (CPB) and a large inductance. By varying the charge n_g induced on the CPB island, we observed oscillations of the device spectrum with the period $\Delta n_g = 2e$. These oscillations are attributed to the charge-controlled AC interference between the fluxon tunneling processes in the CPB Josephson junctions. The measured phase and charge dependences of the frequencies of the $|0\rangle \rightarrow |1\rangle$ and $|0\rangle \rightarrow |2\rangle$ transitions are in good agreement with our numerical simulations. Almost complete suppression of the tunneling due to destructive interference has been observed for the charge $n_g = e(2n + 1)$. The CPB in this regime enables fluxon pairing, which can be used for the development of parity-protected superconducting qubits.

The Aharonov-Casher (AC) effect is a non-local topological effect: the wave function of a neutral particle with magnetic moment moving in two dimensions around a charge acquires a phase shift proportional to the charge [1]. This effect has been observed in experiments with neutrons, atoms, and solid-state semiconductor systems (see, e.g., [2–4] and references therein). Similar effects have been predicted for superconducting networks of nanoscale superconducting islands coupled by Josephson junctions. For example, the wave function of the flux vortices (fluxons) moving in such a network should acquire a phase that depends on the charge on superconducting islands [5]. Indeed, oscillations of the network resistance in the flux-flow regime have been observed as a function of the gate-induced island charge [6]; these oscillations have been attributed to the interference associated with the AC phase. However, this attribution is not unambiguous, because qualitatively similar phenomena can be produced by the Coulomb-blockade effect due to the quantization of charge on the superconducting islands [7].

More recently, indirect evidence for the AC effect in superconducting circuits has been obtained in the study of suppression of the macroscopic phase coherence in one-dimensional (1D) chains of Josephson junctions by quantum fluctuations [8]. The quantum phase slips (QPS) in the junctions can be viewed as the charge-sensitive fluxon tunneling [9, 10] provided the conditions discussed below are satisfied. Microwave experiments [11] have demonstrated that dephasing of a fluxonium, a small Josephson junction shunted by a 1D Josephson chain, can be due to the effect of fluctuating charges on the QPS in the chain. Applications of the AC effect in classical Josephson devices have been discussed in Refs. [7, 12].

In this Letter we describe microwave experiments which provide direct evidence for the charge-dependent interference between the amplitudes of fluxon tunneling. We have studied the microwave resonances of the device consisting of two nominally identical Josephson junctions

separated by a nanoscale superconducting island (the so-called Cooper-pair box, CPB) and a large inductance. A similar device with even greater kinetic inductance provides a physical implementation of the fault tolerant qubit (see below and Ref. [13]). The spectrum of the device is determined by the QPS rate in the CPB junctions, which depends on the charge of the superconducting island. The abrupt change of the phase difference across each junction by $\sim 2\pi$ (see below) can be considered as adding/subtracting a single fluxon to the superconducting loop formed by the CPB and the superinductor. We have observed almost complete suppression of the fluxon tunneling due to the destructive AC interference for the charge on the central CPB island $q = e(2n + 1)$. This complete suppression of fluxon tunneling provides an unequivocal evidence for the Aharonov-Casher phase and clearly distinguishes this effect from the Coulomb-blockade-related effects. Our results obtained for this well-controlled system allow for direct quantitative comparison with the theory.

The studied device (Fig. 1) consists of a superconducting loop that includes a Cooper pair box and a superconducting inductor with a large Josephson inductance L , the so-called superinductor [11]. Below we refer to this loop as the device loop. The magnetic flux Φ in this loop controls the phase difference across the superinductor. The design of our superinductor has been described in Ref. [14]; the superinductor used in this experiment consisted of 36 coupled cells, each cell represented a small superconducting loop interrupted by three larger and one smaller Josephson junctions (Fig. 1b). The inductance L reaches its maximum when the unit cell is threaded by the magnetic flux $\Phi_L = \Phi_0/2$. In this regime of full frustration, L exceeds the Josephson inductance of the CPB junctions by two orders of magnitude.

It is worth emphasizing that a large magnitude of L and, thus, a small value of the superinductor energy $E_L = (\frac{\Phi_0}{2\pi})^2 \frac{1}{L}$, is essential for the observation of the

AC effect in our experiment. Indeed, the classification of the device states by the discrete values of the phase $\varphi = 2\pi m$ and, thus, the notion of fluxons can be justified if $E_L \ll E_J$ because only in this limit one can ignore the phase drop across the CPB (for more details see Supplementary Materials [15]). In this respect, the studied device resembles the fluxonium [16], in which a single junction is shunted by a superinductor. Large inductance L is an important distinction of our device from the structure proposed in Ref. [7] for the observation of suppression of macroscopic quantum tunneling due to the AC effect. In the small- L case considered in Ref. [7], the phase weakly fluctuates around the value $2\pi\frac{\Phi}{\Phi_0}$ and the phase slips are completely suppressed (cf. Ref. [17]). Note that the condition $E_L \ll E_J$ was not satisfied in Ref. [8], so the data interpretation in terms of fluxon tunneling can be questioned. Large L values are also important for the spectroscopic measurements: the superinductor reduces the device resonance frequency down to the convenient-for-measurements 1-10 GHz range.

For the dispersive measurements of the device resonances, a narrow portion of the device loop with the kinetic inductance L_{sh} was coupled to the read-out lumped-element resonator (for details of the readout design, see [18, 19]). The global magnetic field, which determines the fluxes in both the device loop, Φ , and the unit cells of the superinductor, Φ_L , has been generated by a superconducting solenoid. The offset charge on the CPB island was varied by the gate voltage V_g applied to the microstrip transmission line (Fig. 1b).

The device, the readout circuits, and the microwave (MW) transmission line (Fig. 1b) were fabricated using multi-angle electron-beam deposition of Aluminum through a lift-off mask (for fabrication details, see Refs. [18, 19]). Six devices have been fabricated on the same chip; they were addressed individually due to different

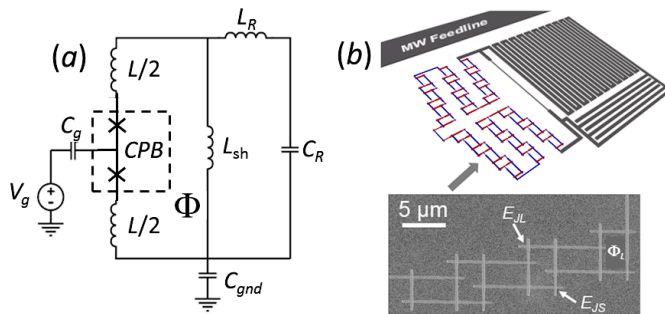


Figure 1. (color online) Panel (a): The schematics of the circuit containing the device and the readout lumped-element resonator. The CPB Josephson junctions are shown as crosses. Panel (b): The layout of the device, the read-out resonator, and the MW transmission line. The superinductor consists of 36 coupled cells, each cell represented a small superconducting loop interrupted by three larger and one smaller Josephson junctions [14].

Table I. Parameters of Josephson junctions in the representative device. Parameters of the CPB junctions correspond to the fitting parameters; parameters of the superinductor junctions were estimated using the Ambegaokar-Baratoff relationship and the resistance of the test junctions fabricated on the same chip.

Junctions	In-plane areas, μm^2	E_J , GHz	E_C , GHz
CPB	0.11×0.11	6	6.4
Superinductor large	0.30×0.30	94	3.3
Superinductor small	0.16×0.16	25	11

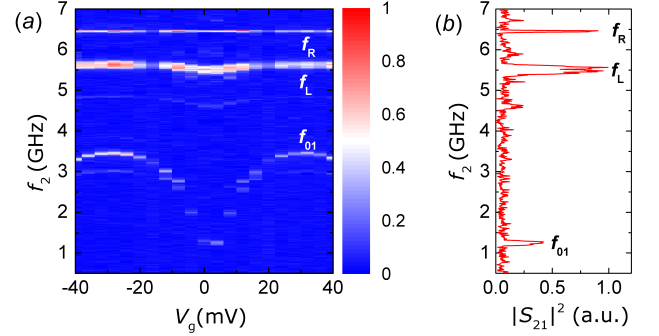


Figure 2. (color online) Panel (a): The transmitted microwave power $|S_{21}|^2$ at the first-tone frequency f_1 as a function of the second-tone frequency f_2 and the gate voltage V_g measured at a fixed value of $\Phi_L = 0.5\Phi_0$. The power maxima correspond to the resonance excitations of the device ($f_2 = f_{01}$), the superinductor (f_L), and the read-out resonator (f_R). Note that the resonance measurements could not be extended below ~ 1 GHz because of a high-pass filter in the second-tone feedline. Panel (b): The frequency dependence of the transmitted microwave power measured at $V_g = 0V$ and $\Phi_{SL} = 0.5\Phi_0$.

resonance frequencies of the read-out resonators. The parameters of the CPB junctions were nominally the same for all six devices, whereas the maximum inductance of the superinductor was systematically varied across six devices by changing the in-plane dimensions of the small junctions in the superinductors [14]. Below we discuss the data for one representative device; Table I summarizes the parameters of junctions in the CPB junctions and superinductor (throughout the Letter all energies are given in the frequency units, $1 K \approx 20.8$ GHz).

In the two-tone measurements, the microwaves at the second-tone frequency f_2 excited the transitions between the $|0\rangle$ and $|1\rangle$ quantum states of the device, which resulted in a change of its impedance [20]. This change was registered as a shift of the resonance of the readout resonator probed with microwaves at the frequency f_1 . The microwave set-up used for these measurements has been described in Refs. [14, 18, 19]. The resonance frequency f_{01} of the transition between the $|0\rangle$ and $|1\rangle$ states was measured as a function of the charge n_g and the flux in the device loop. The f_{01} measurements could not be ex-

tended below ~ 1 GHz because of a high-pass filter in the second-tone feedline.

The results discussed below have been obtained in the magnetic fields that correspond to $\Phi_L \approx \Phi_0/2$ where L reaches its maximum [14]. Because the device loop area ($\sim 1,850\mu m^2$) was much greater than the superinductor unit cell area ($15\mu m^2$), the phase across the chain could be varied at an approximately constant value of L . All measurements have been performed at $T = 20$ mK.

The resonances corresponding to the $|0\rangle \rightarrow |1\rangle$ transition are shown in Fig. 2a as a function of the gate voltage V_g at a fixed value of the magnetic field that is close to full frustration of the superinductor unit cells ($\Phi_L \simeq 0.5\Phi_0$). The dependence $f_{01}(V_g)$ is periodic in the charge on the CPB island, n_g , with the period $\Delta n_g = 1$ (here and below the charge is measured in units $2e \pmod{2e}$). The increase of temperature above 0.3K resulted in reducing the period in half due to the thermally generated quasiparticles population. Figure 2 also shows the resonance of the read-out resonator at $f_R = 6.45$ GHz and the self-resonance of the superinductor $f_L \approx 5.5$ GHz. All three resonances are shown in Fig. 2b for $n_g \approx 0.47$ ($V_g = 0$) and $\Phi_L \approx 0.5\Phi_0$. Weaker resonances observed at $f_2 \approx 3$ GHz and 4.8 GHz at $V_g = -30mV$ correspond to the multi-photon excitations of the higher modes of the superinductor.

Note that no disruption of periodicity neither by the quasiparticle poisoning [21] nor by long-term shifts of the offset charge was observed in the data in Fig. 2a that were measured over 80 min. With respect to the quasiparticle poisoning, this suggests that on average, the parity of quasiparticles on the CPB island remains the same on this time scale. In the opposite case, the so-called “eye” patterns would be observed on the dependences of the resonance frequency on the gate voltage [22]. Significant suppression of quasiparticle poisoning was achieved due to the gap engineering [21] (the superconducting gap in the thin CPB island exceeded that of the thicker leads by $\sim 0.2K$), as well as shielding of the device from infrared photons [23].

The expected flux dependence of the energy levels of the device is shown in Fig. 3a. This flux dependence can be understood by noting that in the absence of fluxon tunneling (the dotted curves in Fig. 3a corresponding to $n_g = 0.5$ and identical CPB junctions) different states are characterized by a different number m of fluxons in the device loop. At $E_J \gg E_L$ the energies of these states are represented by crossing parabolas $E_L(m, \Phi) = \frac{1}{2}E_L(m - \frac{\Phi}{\Phi_0})^2$. The phase slip processes mix the states with different numbers of fluxons and lead to the level repulsion. The qualitative picture of fluxon tunneling and AC interference is in good agreement with the observed level structure shown in Fig. 3b.

Figure 3b shows the main result of this Letter: the dependences of the resonance frequencies of the $|0\rangle \rightarrow |1\rangle$ and $|0\rangle \rightarrow |2\rangle$ transitions (f_{01} and f_{02} , respectively) on

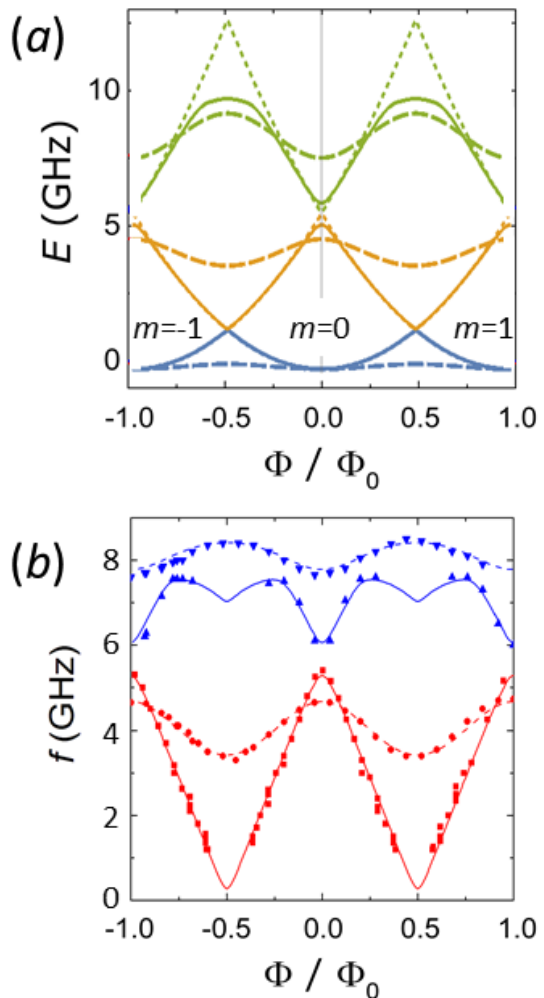


Figure 3. (color online) Panel (a): The flux dependence of the device energy levels obtained by numerical diagonalization of the Hamiltonian (see Supplementary Materials for details, the fitting parameters are listed below). The solid curves correspond to $n_g = 0.5$, the dashed curves - to $n_g = 0$ (the blue curves correspond to the ground state $|0\rangle$, the yellow curves - to the state $|1\rangle$, and the green curves - to the state $|2\rangle$). For comparison we also plotted the dotted curves that correspond to the fully suppressed fluxon tunneling; in this case there are no avoided crossings between the parabolas that represent the superinductor energies $E_L(m, \Phi) = \frac{1}{2}E_L(m - \frac{\Phi}{\Phi_0})^2$ plotted for different m . Panel (b): The dependences of the resonance frequencies f_{01} (red dots - $n_g = 0$, red squares - $n_g = 0.5$) and f_{02} (blue down-triangles - $n_g = 0$, blue up-triangles - $n_g = 0.5$) on the flux in the device loop. The theoretical fits (solid curves - $n_g = 0.5$, dashed curves - $n_g = 0$) were calculated with the following parameters: $E_J = 6.25$ GHz, the asymmetry between the CPB junctions $\Delta E_J = 0.5$ GHz, $E_C = 6.7$ GHz, $E_L = 0.4$ GHz ($L = (\frac{\Phi_0}{2\pi})^2/E_L \approx 0.4\mu H$), $E_{CL} = 5$ GHz.

the flux in the device loop for the charges $n_g = 0$ and 0.5 . In line with the level modeling, at $n_g = 0$ the frequency f_{01} periodically varies as a function of phase, but never approaches zero. On the other hand, when $n_g = 0.5$, the amplitudes of fluxon tunneling across the CPB junctions acquire the Aharonov-Casher phase difference π . Provided that the CPB junctions are identical, the destructive interference should completely suppress fluxon tunneling, which results in vanishing coupling between the states $|m\rangle$ and $|m \pm 1\rangle$ and disappearance of the avoided crossing. Since the difference $E_L(m, \Phi) - E_L(m \pm 1, \Phi)$ is linear in Φ , the spectrum at $n_g = 0.5$ should acquire the sawtooth shape. This is precisely what has been observed in our experiment. To better fit the experimental data, we have assumed that the Josephson energies are slightly different for the CPB junctions ($\Delta E_J < 0.5$ GHz); for this reason, the minima of the theoretical sawtooth-shaped dependence $f_{01}(\Phi)$ are slightly rounded. Fitting allowed us to extract all relevant energies (see the caption to Fig. 3). The amplitude of the single phase slips does not exceed 0.2 GHz, the amplitude of the double phase slips is 0.4 GHz.

The studied device has the potential to become the building block of the fault tolerant qubit. Namely, it can be used to implement a protected qubit in which two logical states correspond to different parities of fluxons in the device loop, the so-called “flux-pairing” qubit. Two conditions have to be satisfied for the realization of protected states [13]. Firstly, the rate of cotunneling of *pairs* of fluxons should be significantly increased by reducing the ratio E_J/E_C for the CPB junctions. Note that at $n_g = 0.5$, the AC phase for cotunneling of fluxon pairs is 2π and the interference is constructive. In this regime, the CPB represents a “ $\cos(\phi/2)$ ” Josephson element which energy is 4π -periodic (see Supplementary Materials [15]). Secondly, for the proper operation of the flux-pairing qubit, the inductance of the superinductor should be further increased (approximately by an order of magnitude in comparison with the device described above). To satisfy the latter challenging requirement without reducing the superinductor resonance frequency, the parasitic capacitance of the superinductor should be significantly reduced. Such a qubit would not only be characterized by much improved coherence, but, even more importantly, would enable certain fault-tolerant gates [13]. The flux-pairing qubit is dual to a recently realized charge-pairing qubit [19].

To conclude, we have observed the effect of the Aharonov-Casher interference on the spectrum of the Cooper pair box (CPB) shunted by a large inductance. Large values of L ($E_L \ll E_J$) are essential for the observation of the AC effect with the Cooper pair box; in this important respect our devices differ from the earlier proposed structures [7]. We have demonstrated that the amplitudes of the fluxon tunneling through each of the

CPB junctions acquire the relative phase that depends on the CPB island charge n_g . In particular, the phase is equal to $0 \pmod{2\pi}$ at $n_g = 2ne$ and $\pi \pmod{2\pi}$ at $n_g = e(2n + 1)$. The interference between these tunneling processes results in periodic variations of the energy difference between the ground and first excited states of the studied quantum circuit; the period of the oscillations corresponds to $\Delta q = 2e$. The phase slip approximation provides quantitative description of the data and the observed interference pattern evidences the quantum coherent dynamics of our large circuit.

We would like to thank B. Doucot for helpful discussions. The work was supported in part by grants from the Templeton Foundation (40381), the NSF (DMR-1006265), and ARO (W911NF-13-1-0431).

SUPPLEMENTARY MATERIALS

ENERGY SPECTRA OF THE COOPER PAIR BOX SHUNTED BY A LARGE INDUCTANCE.

The device studied in this paper consists of two very different elements: a Cooper pair box (CPB) and a superinductor. The Cooper pair box is described by the quantized value of the charge, or by a phase in the interval $(0, 2\pi)$. At significant CPB charging energy it is convenient to use the former basis. In contrast, the superinductor is characterized by continuous conjugated variables, ϕ (phase across) and q (charge). The Cooper pair tunneling to the CPB island changes its charge by ± 1 ; in the symmetric gauge the phase at the inductor ends is $\pm\phi/2$, so the processes of tunneling from different superinductor ends acquire phase factors $\exp(\pm\phi/2)$. Thus, the full Hamiltonian describing the CPB coupled to the superinductor is

$$H = -E_J (a^+ + a^-) \cos(\phi/2) + 4E_C(n - n_g)^2 + 4E_{CL}q^2 + \frac{1}{2}E_L(\phi - 2\pi\Phi/\Phi_0)^2 \quad (1)$$

where a^\pm are operators that raise (lower) the charge of the CPB island, n_g is the charge induced by the gate, and E_{CL} is the effective charging energy of the superinductor that is due to the capacitors of its junctions and ground capacitance of the whole structure.

The analysis is further simplified for large charging energies $E_C \gg E_J$ which is marginally satisfied in the studied device ($E_J = 0.29$ K, $E_C = 0.31$ K). In this case the Cooper pair tunneling is significant only in the vicinity of the full charge frustration, $n_g = N + 0.5$ where the only relevant charging states are $n = N, N + 1$. In the reduced space Hamiltonian becomes

$$H_R = -E_J \cos(\phi/2) \sigma^x + 4E_C(n_g - 0.5) \sigma^z + 4E_{CL}q^2 + \frac{1}{2}E_L(\phi - 2\pi\Phi/\Phi_0)^2 \quad (2)$$

Away from the charge frustration ($n_g = 0.5$) the charge fluctuations are small, so that $\sigma^z \approx -1$ in all low energy states. Duality between phase and charge implies that in this situation the phase fluctuations are large. In this approximation the low energy states coincide with those of the oscillator with $\omega_0 = \sqrt{8E_{CL}E_L}$. Charge fluctuations lead to a weak flux dependence of the energies of these states. In the leading order to the perturbation theory the oscillator potential becomes

$$V = \frac{-E_J^2}{4E_C} \cos \phi + \frac{1}{2} E_L (\phi - 2\pi\Phi/\Phi_0)^2$$

that leads to the weak dependence of the oscillator level on the flux $E_{01} = \omega_0 + \delta E \cos 2\pi\Phi/\Phi_0$. This dependence is exactly the one observed experimentally (red data points in Fig. 3b).

In the opposite limit, close to the full frustration, at $|n_g - 0.5| \ll E_J/E_C$, the phase slip amplitude vanishes due to the destructive Aharonov-Casher interference. Formally in this limit one can treat the second term in (2) as perturbation. In the zeroth order of the perturbation theory one obtains two independent sectors characterized by $\sigma^x = \pm 1$ that we shall refer to as even/odd sectors below. Exactly at $n_g = 0.5$ these sectors are completely independent. At $E_J \gtrsim E_{CL} \gg E_L$ in each sector the low energy wavefunctions are localized in the vicinity of points $\phi = 2\pi m$, m being the number of fluxons in the phase loop. The energy spectrum in this case is given by the set of parabolas shown in Fig. 3a. In this approximation the energy levels corresponding to different parabolas cross. The level repulsion between the levels represented by adjacent parabolas is due to the phase slips that vanish at $n_g = 0.5$.

The level repulsion between the levels represented by next nearest parabolas is due to the double phase slips. Formally it is described by the quantum tunneling in the effective potential

$$V(\phi) = \pm E_J \cos(\phi/2) + \frac{1}{2} E_L (\phi - 2\pi\Phi/\Phi_0)^2 \quad (3)$$

It occurs with amplitude

$$t = A(g)g^{1/2} \exp(-g)\omega_p \quad (4)$$

where $g = 4\sqrt{2E_J/E_{CL}}$, $\omega_p = \sqrt{2E_J E_{CL}}$ and $A(g) \approx 0.8$. This tunneling process changes $m \rightarrow m \pm 2$, but does not mix even and odd sectors. In the limit of large $E_J \gg E_{CL}$ the amplitude becomes exponentially small which was the case for the studied device ($g \approx 6$). In this case the transitions due to double phase slips are almost completely suppressed. The energies of the states with different m are quadratic as a function of the flux, exactly at half flux quantum these energies cross. So the energy difference between the ground and first excited states is linear in Φ with zero intercept. This is exactly the behavior observed in the data (Fig. 3b).

Note that the classification of states by the discrete values of the phase is only possible if $E_L \ll E_J$. In the opposite limit $E_L \geq E_J$ the phase experiences small oscillations around $2\pi\Phi/\Phi_0$ and the phase slips are completely suppressed. In the intermediate regime the phase is localized around the minima of the potential energy $V(\phi)$ that differ from each other by a non-integer fraction of 2π .

The linearity of $E_{01}(\Phi)$ at $n_g = 0.5$ is disturbed by two factors. The first one is the difference in E_J of two junctions comprising the CPB. Due to this difference the flux tunneling is not completely suppressed even at $n_g = 0.5$. This leads to the level repulsion at half integer flux at which neighboring parabolas intersect. This would lead to some rounding of $E_{01}(\Phi)$ around half integer flux. Within the experimental accuracy, the data do not show such effect which implies that the difference between two E_J is small. The second factor is more interesting, it is due to a significant tunneling rate of two fluxons through the CPB. This leads to the level repulsion between the levels corresponding to next neighboring parabolas in Fig. 3a and rounding of the maxima of the spectra data at $n_g = 0.5$ (blue points in Fig. 3b). Some hint of this behavior can be seen in the data, we estimate that $t \approx 0.2$ GHz.

The analytical results obtained above become quantitatively correct in the regime $E_C \gg E_J$ but they remain qualitatively correct even for $E_C \gtrsim E_J$. For more precise quantitative description of the experiment in this regime we used numerical diagonalization of the full Hamiltonian (1). This allowed us to obtain the spectra for all values of the induced charges, n_g , and unambiguous data fit. We found that for the experimental device parameters it is sufficient to restrict oneself to the three lowest energy charging states and range of $\phi = (-12\pi, 12\pi)$. In this approximation the Hamiltonian becomes $3M \times 3M$ matrix where M is the number of discrete values that were used to approximate the continuous variable ϕ . Very accurate results can be achieved by using 0.2π increments (i.e. 20 steps for 4π period).

QUANTUM STATE PROTECTION EXPECTED FOR LARGE INDUCTANCE.

We now briefly discuss the behavior expected for significant double flux tunneling and very large inductance, at which, as we now show, one expects protection against both the charge and flux noise. Generally, tunneling between the states with different m implies that the full wave function is the superposition of the states with different m that can be found from the diagonalization of

the discrete oscillator Hamiltonian

$$H_o = -t(|m\rangle\langle m+2| + |m+2\rangle\langle m|) + 2\pi^2 E_L \left(m - \frac{\Phi}{\Phi_0}\right)^2 \quad (5)$$

where m corresponds to either even or odd numbers. At large $t \gg E_L$ the low energy states in each sector are spread over many different m and are almost indistinguishable. This implies the protection against the external noises. More quantitatively, the dependence on m_0 is given by

$$E(m_0) = 2A(G)G^{1/2} \exp(-G)\Omega \cos(2\pi m_0) \quad (6)$$

$$G = \frac{2}{\pi} \sqrt{\frac{2t}{E_L}} \quad (7)$$

$$\Omega = 4\pi \sqrt{2tE_L} \quad (8)$$

This dependence becomes exponentially small at $G \gg 1$ that indicates weak sensitivity to external flux.

The charge noise can be described as $n_g(t)$ variations. Non-zero value of $n_g - 0.5$ results in a small amplitude that mixes even and odd sectors. This amplitude is given by

$$t_{eo} \approx \pi^{3/4} g^{1/4} E_C (n_g - 0.5) \sqrt{\frac{t}{\omega_p}} \quad (9)$$

Exactly at $\Phi = \Phi_0/2$ the energies of the odd and even sectors become equal in the absence of t_{eo} . Non-zero t_{eo} leads to level splitting but the effect is small in $n_g - 0.5$ and (t/ω_p) .

The equations (6-9) allow one to derive the conditions for optimal charge and flux protection. Generally, the coupling to the charge noise is largest at $\Phi = \Phi_0/2$ because $E_{01} = 2t_m \sim (n_g - 0.5)$ but this coupling becomes small at $t \ll \omega_p$. The flux noise affects the energy levels via $m_0(\Phi)$ dependence. This effect becomes small at $t \gg E_L$. Thus, the optimal protection against the noises is achieved for $\omega_p \gg t \gg E_L$. Notice that while the first inequality is easy to achieve, the second requires a large superinductance. For instance in this experiment $t/E_L \approx 0.05 - 0.5$. For significant protection against flux noise t/E_L should be greater than 10, while for the good charge noise protection one needs $\omega_p/t \gtrsim 10^2$ that results in the condition $\omega_p/E_L \gtrsim 10^3$.

-
- [1] Y. Aharonov and A. Casher, Phys. Rev. Lett. **53**, 319 (1984).
 - [2] A. Cimmino, G. Opat, A. Klein, H. Kaiser, S. Werner, M. Arif, and R. Clothier, Phys. Rev. Lett. **63**, 380 (1989).
 - [3] K. Sangster, E. A. Hinds, S. M. Barnett, and E. Riis, Phys. Rev. Lett. **71**, 3641 (1993).
 - [4] M. Koenig, A. Tschetschetkin, E. M. Hankiewicz, J. Sinova, V. Hock, V. Daumer, M. Schaefer, C. R. Becker, H. Buhmann, and L. W. Molenkamp, Phys. Rev. Lett. **96**, 076804 (2006).
 - [5] B. Reznik and Y. Aharonov, Phys. Rev. D **40**, 4178 (1989).
 - [6] W. J. Elion, J. J. Wachtters, L. L. Sohn, and J. E. Mooij, Phys. Rev. Lett. **71**, 2311 (1993).
 - [7] J. R. Friedman and D. V. Averin, Phys. Rev. Lett. **88**, 050403 (2002).
 - [8] I. M. Pop, B. Doucot, L. Ioffe, I. Protopopov, F. Lecocq, I. Matei, O. Buisson, and W. Guichard, Phys. Rev. B **85**, 094503 (2012).
 - [9] I. M. Pop, I. Protopopov, F. Lecocq, Z. Peng, B. Panetier, O. Buisson, and W. Guichard, Nature Physics **6**, 589 (2010).
 - [10] K. A. Matveev, A. I. Larkin, and L. I. Glazman, Phys. Rev. Lett. **89**, 096802 (2002).
 - [11] V. E. Manucharyan, N. A. Masluk, A. Kamal, J. Koch, L. I. Glazman, and M. H. Devoret, Phys. Rev. B **85**, 024521 (2012).
 - [12] T. T. Hongisto and A. B. Zorin, Phys. Rev. Lett. **108**, 097001 (2012).
 - [13] B. Doucot and L. B. Ioffe, Reports on progress in physics. Physical Society (Great Britain) **75**, 072001 (2012).
 - [14] M. T. Bell, I. A. Sadovskyy, L. B. Ioffe, A. Y. Kitaev, and M. E. Gershenson, Phys. Rev. Lett. **109**, 137003 (2012).
 - [15] *Supplemental Material*.
 - [16] V. E. Manucharyan, J. Koch, L. I. Glazman, and M. H. Devoret, Science **326**, 113 (2009).
 - [17] A. M. van den Brink, arXiv: cond-mat /0206218 (2003), 0206218.
 - [18] M. T. Bell, L. B. Ioffe, and M. E. Gershenson, Phys. Rev. B **86**, 144512 (2012).
 - [19] M. T. Bell, J. Paramanandam, L. B. Ioffe, and M. E. Gershenson, Phys. Rev. Lett. **112**, 167001 (2014).
 - [20] A. Wallraff, D. I. Schuster, A. Blais, L. Frunzio, R.-S. Huang, J. Majer, S. Kumar, S. M. Girvin, and R. J. Schoelkopf, Nature **431**, 162 (2004).
 - [21] J. Aumentado, M. W. Keller, J. M. Martinis, and M. H. Devoret, Phys. Rev. Lett. **92**, 066802 (2004).
 - [22] L. Sun, L. DiCarlo, M. D. Reed, G. Catelani, L. S. Bishop, D. I. Schuster, B. R. Johnson, G. A. Yang, L. Frunzio, L. Glazman, et al., Phys. Rev. Lett. **108**, 230509 (2012).
 - [23] R. Barends, J. Wenner, M. Lenander, Y. Chen, R. C. Bialczak, J. Kelly, E. Lucero, P. O'Malley, M. Mariantoni, D. Sank, et al., Appl. Phys. Lett. **99**, 113507 (2011).